Nfatc1 orchestrates aging in hair follicle stem cells

Brice E. Keyes[a,b], Jeremy P. Segal[a,1], Evan Heller[a,b], Wen-Hui Lien[a,2], Chiung-Ying Chang[a,b], Xingyi Guo[c,3], Dan S. Oristian[a,b], Deyou Zheng[d], and Elaine Fuchs[a,b,4]

[a]Laboratory of Mammalian Cell Biology and Development and [b]Howard Hughes Medical Institute, The Rockefeller University, New York, NY 10065; and [c]Department of Neurology and [d]Departments of Neurology, Genetics, and Neuroscience, Albert Einstein College of Medicine, Bronx, NY 10461

Contributed by Elaine Fuchs, October 30, 2013 (sent for review October 8, 2013)

Hair production is fueled by stem cells (SCs), which transition between cyclical bouts of rest and activity. Here, we explore why hair growth wanes with age. We show that aged hair follicle SCs (HFSCs) in mice exhibit enhanced resting and abbreviated growth phases and are delayed in response to tissue-regenerating cues. Aged HFSCs are poor at initiating proliferation and show diminished self-renewing capacity upon extensive use. Only modestly restored by parabiosis, these features are rooted in elevated cell-intrinsic sensitivity and local elevation in bone morphogenic protein (BMP) signaling. Transcriptional profiling presents differences consistent with defects in aged HFSC activation. Notably, BMP-/calcium-regulated, nuclear factor of activated T-cell c1 (NFATc1) in HFSCs becomes recalcitrant to its normal down-regulating cues, and NFATc1 ChIP-sequencing analyses reveal a marked enrichment of NFATc1 target genes within the age-related signature. Moreover, aged HFSCs display more youthful levels of hair regeneration when BMP and/or NFATc1 are inhibited. These results provide unique insights into how skin SCs age.

BMP signaling | hair cycle | quiescence

In adult tissues, stem cells (SCs) must replace cells lost to acute injury and normal biological activity (homeostasis). Aging can be viewed as a failure to maintain proper tissue homeostasis, resulting in a decline in tissue function and delayed response to tissue damage (1). Age-related extrinsic changes in external, systemic, and/or local tissue environment, coupled with intrinsic changes from repetitive use, are all potential underlying causes for SC malfunction. However, the relative contributions of these factors on SC aging vary among SC populations. Studies on hematopoietic and melanocyte SCs show that age-related intrinsic perturbations can impair SC function (2–4). Mesenchymal SCs, cardiac SCs, and liver progenitor cells also show age-related declines in performance (5–7). The impact of extrinsic perturbations is evident from studies on muscle and neural SCs, where exposure to a youthful systemic environment can restore SC functional capabilities (7–10). Most recently, it was shown that cardiomyocytes rely upon systemic growth and differentiation factor 11 (GDF11), a member of the transforming growth factor β (TGF-β) superfamily, which declines with age (11).

The skin has some of the most recognizable age-associated changes. In humans and other mammals, skin shows an age-related decline in homeostasis, with both dermal and epidermal thinning, reductions in epidermal proliferation and injury repair, loss of dermal elasticity, wrinkling, and notably, hair thinning and eventual loss (12). Periods of rest in hair follicles (HFs) also become longer as animals age, and in humans, hair density declines with age. It has been suggested that the progressive dormancy of HFs during aging is a reflection of a declining capacity of SCs to initiate a new hair cycle, but this has not been formally tested and the underlying mechanisms remain largely unexplored.

HFs undergo cyclic rounds of growth (anagen), degeneration (catagen), and rest (telogen), termed the "hair cycle" (13). During anagen, HFs regenerate and develop into mature HFs. In close association with the dermal papilla at the base of the mature follicle, transit-amplifying matrix cells proliferate rapidly and then progress to terminally differentiate to form the hair shaft and its channel. At the start of catagen, most cells in the lower two-thirds of the follicle are eliminated by apoptosis, and the dermal papilla regresses. It stops when it reaches the base of the noncycling portion of the HF, a region referred to as the "bulge." HFs then enter the dormant telogen phase of the hair cycle, which gets longer with aging.

A critical component of anagen is the activity of HFSCs, which drive these cyclical rounds of HF regeneration (13). Several studies have shown that the bulge region within the HF is a niche for HFSCs, with the majority of label retaining/slow cycling cells found in the bulge after pulse-chase experiments (14, 15). When isolated and placed in vitro, bulge cells initiate colonies; over time, a few grow to large holoclones, consisting of small, undifferentiated cells with long-term proliferative potential; cells from holoclones also exhibit multipotency when engrafted onto *Nude* mice in vivo (16). Lineage tracing studies show that cells within the bulge and/or its base (hair germ) fuel the hair cycle (17–19).

The identification of a population of adult HFSCs that can regenerate hair has led to their purification and molecular characterization. Transcriptional profiling shows that HFSCs preferentially express a set of highly enriched (signature) genes, including transcription factors [*Sox9*, *Tbx1*, *Lhx2*, *TCF3/4*, and nuclear factor of activated T-cell c1 (*NFATc1*)], that maintain them in a quiescent, undifferentiated state (15, 17). HFSCs remain quiescent until the next wave of HF regeneration is initiated. A new hair cycle begins when the balance of Wnt-activating and bone

Significance

Signs of aging often first appear in our skin and hair. As animals age, hair follicles spend more time resting instead of generating hair. Here we show that this decline is rooted in age-related changes in systemic, local, and intrinsic factors, which collaborate to reduce hair follicle stem cell (HFSC) activity. We uncover a unique and hitherto-undescribed age-related role for bone morphogenic protein signaling and a downstream effector, nuclear factor of activated T-cell c1 (NFATc1). In young stem cells, NFATc1 is on when they are quiescent and wanes when they make hair. In aging follicles, NFATc1 and its target genes remain high too long. Importantly, NFATc1 inhibitors restore youthful behavior to aging HFSCs, providing unique insights into age-related changes in skin physiology.

Author contributions: B.E.K., J.P.S., W.-H.L., D.Z., and E.F. designed research; B.E.K., W.-H.L., C.-Y.C., and D.S.O. performed research; J.P.S. and E.H. contributed new reagents/analytic tools; B.E.K., J.P.S., W.-H.L., X.G., D.Z., and E.F. analyzed data; and B.E.K. and E.F. wrote the paper.

The authors declare no conflict of interest.

Freely available online through the PNAS open access option.

Data deposition: The raw ChIP sequencing data have been deposited in the Gene Expression Omnibus database, www.ncbi.nlm.nih.gov/geo (accession nos. GSE52328 and GSE48878).

[1]Present address: Biological Sciences Division, Department of Pathology, The University of Chicago, Chicago, IL 60637.

[2]Present address: de Duve Institute, Université Catholique de Louvain, B-1200 Brussels, Belgium.

[3]Present address: Department of Biomedical Informatics, Vanderbilt University School of Medicine, Nashville, TN 37240.

[4]To whom correspondence should be addressed. E-mail: fuchslb@rockefeller.edu.

This article contains supporting information online at www.pnas.org/lookup/suppl/doi:10.1073/pnas.1320301110/-/DCSupplemental.

morphogenic protein (BMP)-inhibitory cues from the SC niche and surrounding dermis is shifted (19–21). Sensitive to BMP signaling for its transcription and calcium for its nuclear localization, NFATc1 is among the quickest to respond, being downregulated/lost upon HFSC activation and fate commitment (22, 23).

In this study, we focus on how HFSCs change as they age and how this contributes to the phenotypic and hair cycle-related features of aging skin. Using a mouse model, we show that aged HFSCs are considerably more quiescent than young HFSCs, and they are more difficult to activate, resulting in significantly more sluggish entry into anagen. In vitro, the most striking defect in aged HFSCs is their reduced colony-forming efficiency (CFE). Aged HFSC holoclones that do grow can be passaged, but show signs of diminished self-renewal in later passages. Intriguingly, the CFE defect can be partially rescued by plating HFSCs from aged HFs that have been depilated, a process known to reduce BMP6 and fibroblast growth factor 18 (FGF18) niche levels (19). Age-related differences in systemic factors have modest impact relative to local and intrinsic changes in BMP signaling/sensitivity. Digging deeper, we use transcriptional profiling and ChIP sequencing (seq) analyses to unearth key age-related perturbations in BMP-/calcium-mediated regulation of NFATc1, which when rectified, restore transcriptional and physiological features of aged HFSCs to their youthful state.

Results

HFs Become Increasingly Dormant with Age. We set out to examine what effects age would have on the regenerative process of the hair cycle and the relationship to possible changes in HFSC functionality with age. When HFs enter anagen in C57BL/6 mice, the skin transitions from pink to black, reflecting the coactivation and differentiation of melanocyte SCs resident in HFs from Anagen IIIa until catagen (24). As judged by this and histological analyses, the first two hair cycles in C57BL/6 mice were largely synchronous, reflecting the ability of neighboring HFs to coordinate HFSC activities (25). Thereafter, hair growth became increasingly asynchronous (26) such that by the ∼eighth hair cycle, aged mice (defined here as animals 22–24 mo of age) displayed discrete domains of anagen-phase HFs (black) interspersed with large patches of telogen-phase (pink) skin (Fig. 1*A*). This patchiness was not attributable to age-related changes in melanocyte differentiation, as the numbers of melanocyte SCs within the bulge of telogen-phase HFs did not change with age (*SI Appendix*, Fig. S1*A*), nor did the numbers of differentiated melanocytes within the hair bulb of anagen-phase HFs (*SI Appendix*, Fig. S1*B*), and hair shaft pigmentation was unaffected (*SI Appendix*, Fig. S1*C*). Rather it was a faithful indicator of whether HFs were in the telogen phase or anagen phase.

Using this assay, we next monitored hair cycle progression for 100–200 d in cohorts of young and aged animals (*SI Appendix*, Fig. S1 *D–F*). Quantifications revealed that although aged HFs cycle, the percentage of the area of HFs entering anagen undergoes a dramatic decline with age (94 ± 4% to 21 ± 10%, P = 0.005) (Fig. 1*B*). As summarized by heat map, the skins of young animals (defined here as animals 2–4 mo of age) repeatedly and synchronously entered anagen during the observation interval (Fig. 1*C*). By contrast, very few HFs of aged mice cycled more than once, and many HFs never entered anagen during this time (Fig. 1*C*). We also observed ∼threefold more independent anagen domains during a single hair cycle in aged skin (6.1 ± 0.8 to 1.9 ± 0.2 domains), reflecting the increasingly asynchronous, regional domain-based activation of HFs.

To probe more deeply into the age-related differences in HF cycling, we quantified durations of anagen and telogen within regionally matched subdomains of HF activity from young and aged mice. These analyses revealed that aged HFs spend more than twice as long in the telogen phase as their younger counterparts (92 ± 3 d vs. 43 ± 1 d) (Fig. 1*D*). Even more noteworthy was a corresponding shortening of the anagen phase of aged HFs (10 ± 1 d vs. 16 ± 1 d) (Fig. 1*E*). The outcome of these age-related differences was an overall shorter hair coat (Fig. 1*F*) with a sparser and more ragged appearance. Together, these data show that in aged animals, the HFs of the dorsal coat are more dormant, staying in telogen for longer periods of time and are punctuated by shorter periods of anagen.

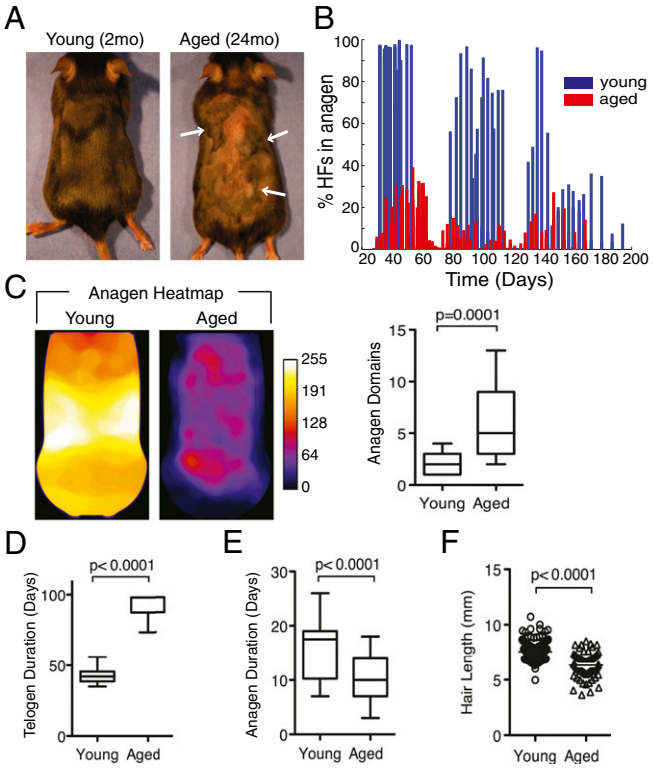

Fig. 1. Hair cycle dynamics in aged animals. (*A*) Representative images of young and aged animals with hair clipped (shaved) during anagen. Arrows point to domains of anagen growth on aged animal. (*B*) Quantification of the cumulative percentage of back skin area that enters anagen in young (blue bars) and aged (red bars). n = 7 aged animals; n = 8 young animals. (*C*, *Left*) Heat map showing overlay of anagen from all animals observed. Warm colors (yellow/white) signify areas of highest anagen activity and cool colors (purple/blue) areas of low activity. (*C*, *Right*) Quantification of the number of individual domains present during a single anagen cycle in young and aged animals. Data are mean ± SEM. Quantification of time discrete areas of back skin spend in telogen (*D*) and anagen (*E*), and length of individual awl hairs from young and aged animals (*F*). Data are mean ± SEM.

Aged HFSCs Have a Delayed Response to Activation Cues. To further explore the underlying cause for age-related regional variation in hair cycling, we asked whether this might be rescued by depilation (hair plucking by waxing), a procedure that stimulates telogen HFs of young mice to enter anagen. Both in young and aged mice, depilation removes not only the hair shafts (club hairs), but also an inner bulge layer of BMP6- and FGF18-expressing cells that otherwise poses a high threshold for activation of the outer bulge layer of quiescent HFSCs (19). The skin of young and aged animals was monitored for appearance of skin pigmentation after depilation.

In the representative young animal (2 mo of age) shown in Fig. 2*A*, early telogen-phase HFs entered anagen within ∼5 d post-depilation, rather than ∼20 d without depilation (Fig. 1*B*). As judged by pink→black skin transitions, HFs in the representative aged animal (24 mo of age) responded and in a much more synchronous fashion than their nondepilated counterparts, suggesting that local niche signals might in part underlie age-related asynchrony. That said, anagen entry was clearly delayed by several days in aged vs. young mice (Fig. 2*A*).

To examine the kinetics of HFSC activation after depilation, we used a series of 5-ethynyl-2′-deoxyuridine (EdU) labeling ex-

periments to determine when HFSCs were proliferating after depilation (Fig. 2*B*). We examined EdU incorporation from 24 to 96 h after depilation, as this has been previously shown to be when HFSCs proliferate during anagen (27). EdU was administered by i.p. injection twice daily every 12 h in groups of animals from 24 to 48 h (early pulse), 48–72 h (mid-pulse), 72–96 h (late pulse), and 0–96 h (continuous pulse). EdU incorporation in HFSCs ($CD34^{high}\alpha6\text{-integrin}^{high}$) was quantified by fluorescence-activated cell sorting (FACS) for each time point.

As judged by the incorporation of EdU, fewer aged HFSCs were induced to proliferate in the early stage after depilation (11 ± 2.5% compared with 31 ± 4.2% EdU^+ HFSCs) (Fig. 2 *B* and *C*). EdU incorporations from mid- to late pulses were similar. However, HFSC proliferation throughout anagen (total EdU incorporation after 4 d of labeling) was decreased in aged HFSCs (39 ± 1.0% compared with 55 ± 3.0% EdU^+ HFSCs) (Fig. 2*D*). When monitored at 4-mo intervals, cycling was sustained up until 12 mo of age, when EdU incorporation began to drop (*SI Appendix*, Fig. S2*A*). This decline did not appear to be reflective of elevated apoptosis, as activated caspase3 immunolabeling was comparable in aged and young HFs (*SI Appendix*, Fig. S2*B*). Together, these results pointed to an age-related delay in HFSC activation following depilation. These results further suggested that aged HFSCs may have an intrinsically higher threshold for activation than younger HFSCs.

Aged HFSCs Are More Sensitive to BMP Signaling in Vitro and in Vivo. To test for possible intrinsic differences in HFSC activation, we began by using FACS to purify HFSCs on the basis of surface markers CD34 and integrin-α6 (16). Analysis of FACS profiles indicated that HFs in aged and young mice contained equivalent numbers of HFSCs, similar to what has been reported for epidermal SCs (28) (*SI Appendix*, Fig. S2*C*). Immunolabeling and quantifications for additional HFSC markers corroborated this similarity (*SI Appendix*, Fig. S2 *D* and *E*). Upon culture, however, aged HFSCs grew more slowly and formed significantly fewer colonies than young HFSCs (1.6 ± 0.4 vs. 10 ± 1.0 colonies per 10^4 cells) (Fig. 3 *A* and *B*; *SI Appendix*, S3 *A–C*). This decline in CFE surfaced by 12 mo of age and progressed thereafter (*SI Appendix*, Fig. S3 *D–G*). Overall, our findings were in good agreement with prior studies reporting an age-related decline in SC colony formation in vitro (29–31).

Aged and young HFSCs adhered comparably, ruling this out as the basis of the defect in CFE (*SI Appendix*, Fig. S3*H*). Moreover, when plating 10^4–10^5 aged HFSCs, colony-forming efficiencies followed a linear trend, ruling out a density-dependent contribution to differences in plating efficiencies (*SI Appendix*, Fig. S3*I*). Digging deeper, we discovered that only a few aged HFSC colonies grew to the typical size of holoclones [10–30 mm^2, 2×10^4 to 5×10^4 cells (32)] (*SI Appendix*, Fig. S3*J*). Even the average size was smaller for aged vs. young colonies (8.5 ± 2.0 mm^2 vs. 22 ± 1.9 mm^2) (Fig. 3*B*). Nevertheless, most of the cells within the aged colonies were tightly packed and undifferentiated, which are both hallmarks of clones derived from SCs (Fig. 3*A*, *Lower*). Moreover, when colonies were picked and passaged, they gave rise to colonies in the normal numbers and sizes of their younger counterparts (Fig. 3*C*). It was only after 10 rounds of passaging that we observed a decrease in the self-renewal capacity of aged HFSCs (Fig. 3*D*). Taken together, despite their equivalence in numbers between 2 and 24 mo and their equivalent adhesion, aged HFSCs do not proliferate in vitro as effectively or as long term as young SCs.

To pursue these differences further, we cultured young and aged HFSCs following depilation (Fig. 3*E*). Activated HFSCs (aHFSCs) from young and aged animals both formed colonies with ~10-fold improved efficiencies. Quantifications revealed that CFE was reduced from a 10-fold difference in telogen to only twofold difference for aged vs. young HFSCs postdepilation (11 ± 1.1 aged to 19 ± 3.1 young colonies 48 h postdepilation, 13 ± 2.2 aged to 27 ± 3.0 young colonies 72 h postdepilation) (Fig. 3*F*). Moreover, differences in colony size were restored to youthful

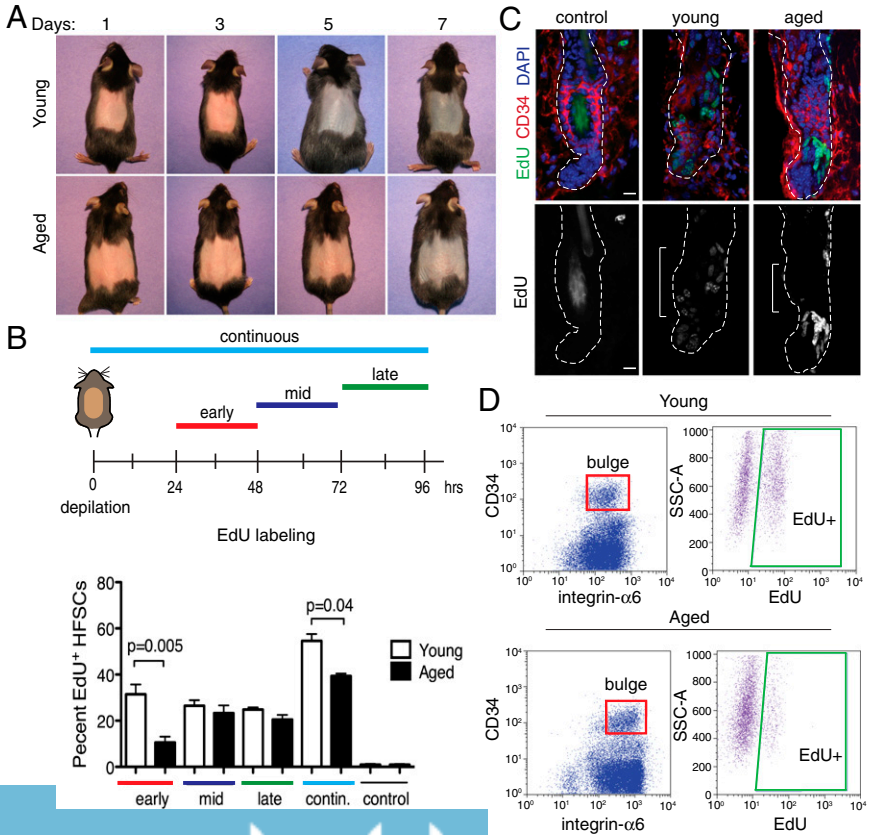

Fig. 2. HFSC activation is delayed in aged animals. (*A*) Representative images of a young (*Upper*) and aged (*Lower*) animal 1, 3, 5, and 7 d after depilation. (*B*) Schematic diagram illustrates experimental design of depilation experiments (*Upper*). Quantifications of EdU incorporation (*Lower*) in the bulge at indicated time points by flow cytometry. $n = 4$ early/mid-; $n = 2$ late/continuous; $n = 3$ controls. Data are mean ± SEM (*C*) EdU incorporation in HFSCs after depilation. Merge image (*Upper*) of control (no depilation) and young and aged HFs. CD34 staining marks the bulge. EdU staining alone (*Lower*), bracket denotes the bulge area. (Scale bar, 10 μM.) (*D*) Representative FACS plots used for quantifying EdU incorporation into the bulge after depilation.

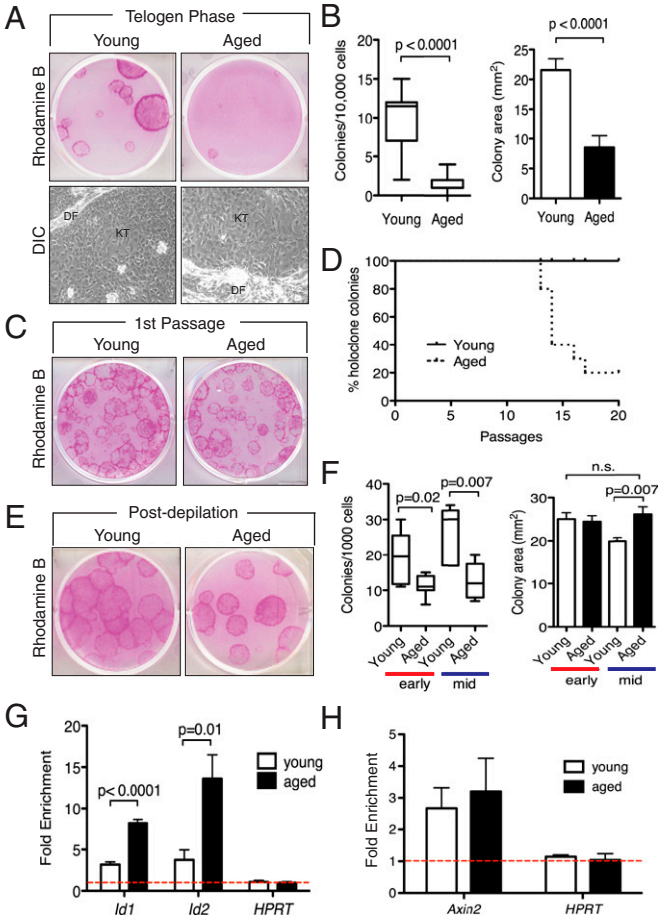

Fig. 3. Aged HFSC function is diminished in vitro. (*A*, *Upper*) CFE from telogen-phase back skins. Colonies from FACS-isolated young and aged HFSCs are stained with Rhodamine B. (*A*, *Lower*) Differential interference contrast (DIC) images of cells within colonies. Note the small, compact, and undifferentiated cells within the colony. DF, dermal fibroblast; KT, keratinocyte. (*B*) Quantification of CFE and colony sizes (in mm^2). $n = 5$ young; $n = 4$ aged. Data are mean ± SEM (*C*) Image of young and aged colony formation after first passage in vitro. (*D*) Long-term passage ability of young and aged HFSCs. Data are presented as percent holoclones formation. $n = 10$ colonies for each group. (*E*) CFE after depilation at specified time points. Colonies from FACS-isolated young and aged HFSCs stained with Rhodamine B. (*F*) Quantification of CFE and colony size. $n = 4$ for both groups. Data are mean ± SEM (*G*) qRT-PCR for *Id1* and *Id2* after BMP4 treatment of HFSC colonies in vitro. $n = 4$ for each group. Data are mean ± SEM. (*H*) qRT-PCR for *Axin2* and *HPRT* after WNT3a treatment of HFSC colonies in vitro. $n = 4$ for each group. Red dashed line denotes the level above which expression is enriched. Data are mean ± SEM.

levels by depilation (25 ± 1.5 mm^2 to 24 ± 1.3 mm^2 at 48 h postdepilation, but 20 ± 0.8 mm^2 to 26 ± 1.7 mm^2 by 72 h postdepilation). We attribute the slight reduction in colony size in the young mid-time point to the large number of colonies formed in the assay. These results suggest that aged HFSCs can be activated to proliferate but require a stronger stimulus to do so. Because HFSC activation requires inhibition of BMP signaling and enhanced Wnt signaling, we tested their effects in our cultures. As shown in Fig. 3 *G* and *H*, aged HFSCs were intrinsically more sensitive to BMP4 than younger HFSCs, as judged by levels of inhibitor of DNA binding 1 (*Id1*) and *Id2* expression, established downstream targets of activated BMP signaling, as a readout of BMP signaling responsiveness. In contrast, they showed no difference in response to WNT3A, as judged by expression of the highly sensitive Wnt target gene, *Axin2*. This finding is in agreement with the depilation experiment, as depilation is known to stimulate HFSC activation in part by reducing BMP6 levels in the niche (19).

Given the heightened sensitivity of aged HFSCs to BMP signaling and their improved colony-forming ability when cultured from a bulge exposed to a depilation-induced reduction in BMPs, we turned to addressing whether BMP signaling is elevated in aged HFSCs in vivo. Postdepilation analyses revealed that in contrast to young HFSCs, which down-regulated phospho-SMAD1/5/8 (pSMAD1/5/8) in the bulge, aged HFSCs failed to do so (Fig. 4*A*). This was also true for ID2 (*SI Appendix*, Fig. S4*A*) and similar results were obtained for ID1 (not shown). These data provided compelling evidence that elevated sensitivity to BMP signaling was responsible for keeping aged follicles in a more quiescent state.

Exploring the Impact of Systemic and Local Environment on Aged HFSC Behavior and BMP Signaling. We next addressed whether age-related systemic changes might contribute to the behavior of aged HFSCs, as seen in neural SCs, muscle SCs, and cardiomyocyte systems (7, 9, 11). Using parabiosis, we surgically joined mice so that they shared a circulatory system (12, 33, 34). For this study we established isochronic (young–young and aged–aged) and heterochronic (young–aged) parabiotic pairs of mice to examine the impact of the systemic environment on aged HFSC function (Fig. 4*B*) (13, 35). Eight weeks following surgery, we then isolated and cultured telogen-phase HFSCs (tHFSCs).

While parabiosis did not significantly affect CFE in the young heterochronic mice, it did enhance CFE in aged HFSCs from heterochronic mice (Fig. 4 *C* and *D*). That said, these effects were relatively modest, and colony size was not substantially improved in aged HFSCs cultured from the aged animal of heterochronic vs. isochronic pairs. Additionally, after testing the effects of depilation on this process, we found no differences in CFE or colony size between HFSCs from heterochronic and isochronic aged animals (Fig. 4*E*). Similar results were obtained in vivo, when we examined EdU incorporation and HFSC behavior following depilation of isochronic and heterochronic pairs (not shown). Taken together, these results suggest that the systemic environment is not the major contributing factor to the delay in HFSC activation or the defects in CFE seen in aged HFSCs.

We next turned to addressing the impact of local environment, namely skin epidermis, dermis, and adipose tissue, as possible sources of elevated BMP signaling. As judged by quantitative PCR with reverse transcription (qRT-PCR), *Bmp2*, *Bmp4*, and *Bmp6* but not *Bmp7* mRNAs were significantly elevated in adipose tissue of aged vs. young skin (Fig. 4*F*). There were also minimal increases in *Bmp2* within skin epithelium and in *Bmp6* within both the epithelium and dermis. Consistent with this observation, when young and aged follicles were synchronized by depilation and allowed to enter into competent telogen (40 d after depilation), higher levels of pSMAD1/5/8 and ID2 were detected in the bulge of aged follicles (Fig. 4*G* and *SI Appendix*, Fig. S4*B*). By contrast, no age-related differences were noted in *Wnt* mRNAs (*SI Appendix*, Fig. S4*C*).

When taken together with prior studies showing that dermal BMP4 and BMP6 and adipocyte BMP2 are potent inhibitors of anagen in young mice (20, 23), our results suggested that during aging, local BMP levels rise and powerfully impact HFSC activation. If so, aged HFs would need a larger reduction in BMP signaling in the local environment to initiate anagen. To explore this possibility in greater detail, we reduced the BMP contribution provided by the Keratin 6 inner bulge by plucking different sized areas (1, 1.5, 2, and 3 mm^2) of the telogen-phase skin of aged and young mice. Interestingly, anagen initiation hair regrowth occurred in all of the regions plucked in young animals, whereas hair regrowth in aged mice was only observed if the plucked regions with an area of least 2 mm^2 (Fig. 4 *H* and *I*). Even then, the 2-mm^2 plucked area showed hair regrowth in only 40% of the aged animals tested.

Conversely, we used the BMP antagonist Noggin to titrate the levels of BMP in young and aged HFs. Noggin was injected intradermally into young and aged animals and EdU incorporation

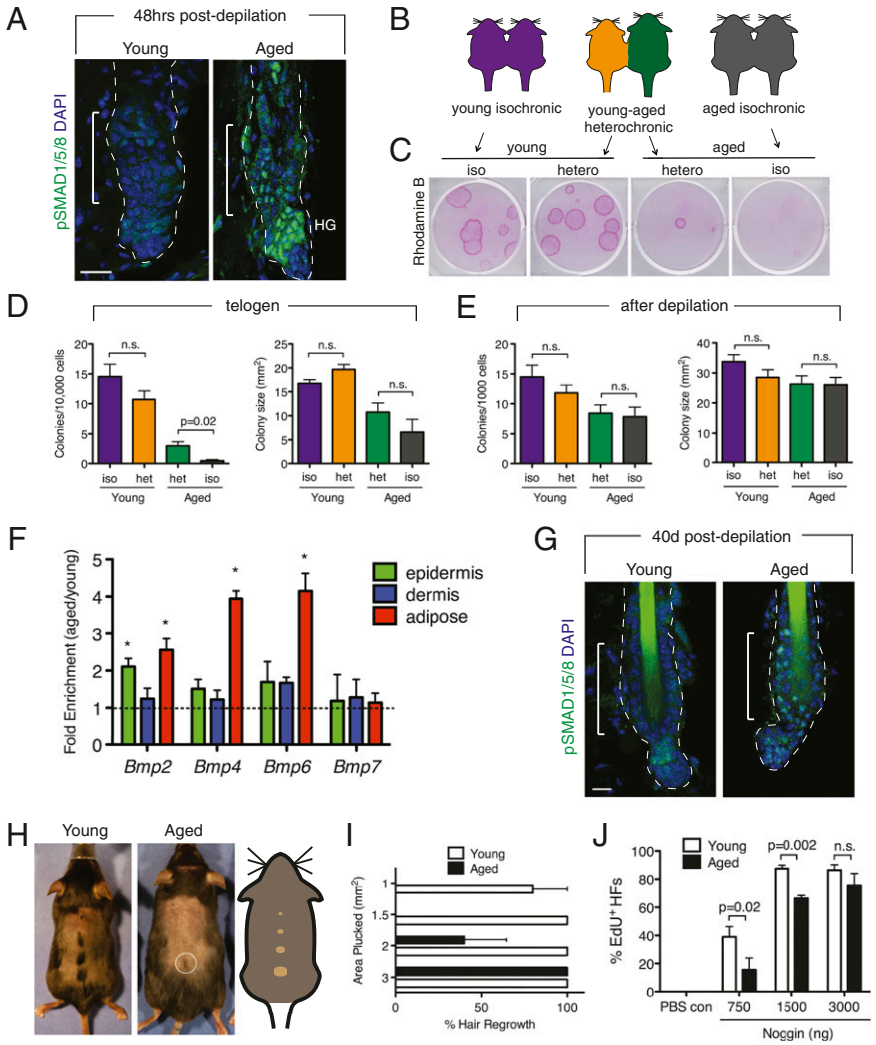

Fig. 4. Systemic and local factors impact on aged HFSCs. (*A*) Images of HFs sectioned and immunostained for pSMAD1/5/8 48 h after depilation. Brackets in young and aged HFs denote the bulge area. HG, hair germ. (Scale bar, 20 μM.) (*B*) Schematic of parabiosis pairs. Isochronic young represents young–young animal pairing, heterochronic represents young–aged animal pairing, and isochronic aged represents aged–aged animal pairing. (*C*) Holoclone forming efficiency of HFSCs from telogen-phase back skins after parabiosis. Colonies from FACS-isolated young and aged HFSCs stained with Rhodamine B. (*D*) Quantification of CFE and colony size. n = 3 isochronic pairs; n = 3 heterochronic pairs. Data are mean ± SEM. n.s., not significant. (*E*) Quantification of CFE and colony size of HFSCs 48 h after depilation after parabiosis. Data are mean ± SEM. (*F*) qRT-PCR for BMPs from whole-tissue lysates. Data are represented as fold enrichment (aged/young). n = 4 for each group. Data are mean ± SEM. $^*P < 0.05$. (*G*) Images of HFs immunostained for pSMAD1/5/8 40 d after depilation. (Scale bar, 20 μM.) (*H*) Representative images of animals after depilation and regrowth of hair (*Left* and circle in *Center*). Areas of hair plucked are indicated on diagram (*Right*). (*I*) Quantification of hair regrowth on young and aged animals. n = 5 young; n = 5 aged. Data are mean ± SEM (*J*) Quantification of HFs with EdU⁺ hair germs after Noggin injection at the indicated levels. n = 3 for each group. Data are mean ± SEM.

in HFs was scored 5 d postinjection. Indeed, a higher dosage of Noggin was necessary to induce similar levels of HF activation in aged and young animals (Fig. 4*J*). These data clearly indicate that local skin environment imposes a higher threshold for activation in aged vs. young animals. Moreover, because plucking the hair can counteract this threshold, our findings are consistent with the notion that the key inhibitory factor restricting HFSC activity in older mice is BMP signaling.

Finally, even though these data showed that age-related changes in dermal and s.c. macroenvironment contribute significantly to differences in aged HFSC behavior, an analysis of age-related differences in the behaviors of the clustered HF triplets of tail skin indicated that additional complexities are involved. In young mice, nearly 50% of clusters displayed three anagen-phase HFs; in aged animals, most clusters contained only a single anagen-phase HF (*SI Appendix*, Fig. S4 *D–F*). These differences offered a unique insight, because in contrast to the regional heterogeneity of aged back-skin follicles, the differences in anagen HFs within closely juxtaposed triplets were not easily explained by putative variations across the dermis. When taken together with the enhanced intrinsic sensitivity of aged HFSCs to BMP signaling, these findings suggest that both intrinsic and extrinsic changes in BMP signaling contribute to the age-related phenotypes we observe here.

aHFSCs of Aged Mice Are More Similar to tHFSCs of Younger Mice than to Young aHFSCs. To explore the molecular mechanisms underlying age-related decline in HFSC function, we used high-throughput RNA sequencing (RNA-seq) to transcriptionally profile young and aged HFSCs in the telogen phase and aHFSCs (48 h postdepilation). The relationship of each cell population to the others was revealed by unsupervised hierarchical clustering algorithms. As shown by heat map, aHFSCs of aged mice were more similar to tHFSCs of younger mice than to young aHFSCs (*SI Appendix*, Fig. S5*A*).

In aged HFSCs, most genes ≥twofold changed following activation were down-regulated relative to their young counterparts (Fig. 5*A*). This cohort included genes encoding extracellular matrix (ECM) proteins, such as lumican, collagens, fibronectin, laminins, and tenascin-C, as well as stefins and cysteine proteases implicated in ECM remodeling (*SI Appendix*, Table S1). These changes, and others involved in cell migration, were consistent with the sluggishness of aged HFSCs in initiating HF down-growth.

Pathway and functional analyses of age-related changes after HFSC activation were consistent with alterations in proliferation and survival (*SI Appendix*, Fig. S5*B*). Moreover, genes preferentially down-regulated in aging were predicted to promote these processes, whereas those that were up-regulated were implicated in suppressing them. Notably, however, we did not find evidence for up-regulation of the *Ink4a/4b* locus encoding p16 and $p19^{ARF}$ stress-response proteins, which are often up-regulated in aging (14, 36, 37).

NFATc1 Is Elevated in Aged HFSCs and Delays Entry into Anagen. Given the transcriptional similarities between depilation-activated aged HFSCs and their young telogen-phase counterparts,

we cross-referenced our differentially expressed transcripts with the bulge signature gene set (transcripts up-regulated in young HFSC versus young epidermal SCs) (15, 23). Interestingly, only 5% of the age-related changes were part of this signature (Fig. 5*B* and *SI Appendix*, Fig. S5*C* and Table S2). Among this small cohort was a sustained signature transcript encoding NFATc1, an established BMP-/calcium-regulated, HFSC transcription factor whose ablation stimulates precocious entry of HFs into anagen (22) (Fig. 5*C*). As judged by immunofluorescence, nuclear NFATc1 was prominent in both young and aged tHFSCs; following depilation, however, nuclear NFATc1 dramatically plummeted in young but not aged HFSCs (Fig. 5*D*).

To test whether elevated nuclear NFATc1 levels might be contributing to the age-related defects in the activation of HFSCs and their entry into anagen, we used the small peptide inhibitor VIVIT, to block NFAT activity. VIVIT inhibits calcineurin-mediated dephosphorylation of NFATc1 proteins and efficiently blocks its nuclear translocation (22, 38). Quantifications revealed that VIVIT erased the significant differences between NFATc1 levels in depilation-induced aged vs. young HFSCs (Fig. 5*E*). By contrast, VIVIT did not dramatically alter NFATc1 levels in young HFSCs, which naturally down-regulate NFATc1 upon depilation. Similarly, whereas VIVIT did not significantly affect the proliferation and activation of young HFSCs, VIVIT profoundly affected proliferation and activation of aged HFSCs 48 h post-depilation (Fig. 5 *F* and *G*). These effects were maintained in vitro, as CFE and colony size were similar between aged and young animals treated with VIVIT and depilation before culture (Fig. 5*H*). Overall, these experiments demonstrate that by inhibiting NFATc1 activity, aged HFSCs restore the activation kinetics and CFE to more youthful levels.

NFATc1 Targets Are Enriched Among Genes That Are Differentially Expressed in Depilation-Activated HFSCs from Aged vs. Young Mice. To determine the extent to which NFATc1 might contribute to the aged HFSC signature, we performed chromatin immunoprecipitation followed by deep sequencing (ChIP-seq) analysis for NFATc1 with FACS-isolated quiescent HFSCs. A total of 3,438 genes bound NFATc1 (~15% of all genes) (*SI Appendix*, Table S3), with peaks enriched in promoter and/or gene proximal regions (*SI Appendix*, Fig. S6 *A* and *B*). The NFATc1 ChIP-seq was specific, as its motif was enriched among the peaks (*SI Appendix*, Fig. S6*C*). Fig. 6*B* shows representative ChIP-seq signal tracks of three NFATc1 target genes in HFSCs. Consistent with NFATc1 expression, ChIP–qRT-PCR confirmed that these genes are significantly enriched in HFSCs (NFATc1$^+$) compared with interfollicular epidermal cells [(IFEs) NFATc1$^-$].

Even more interesting, of the 185 genes that are more highly expressed in depilation-activated aged HFSCs, nearly 40% bound NFATc1 ($P < 0.0001$) (Fig. 6*A*). Moreover, consistent with NFATc1's role as both a transcriptional activator and repressor (39, 40), NFATc1 bound to 19.5% of the 1,180 genes ($P = 0.0001$) which showed lower expression in aged HFSCs than young ones following depilation. This was notable, considering that less than 15% of mouse genes showed NFATc1 binding.

The age-related NFATc1 target genes were enriched for functional annotations, such as epithelial neoplasia and development (up-regulated genes) and cell stimulation, mitosis, and differentiation (down-regulated genes) (*SI Appendix*, Fig. S6*D*). Moreover, this group was significantly enriched for HFSC signature genes ($P < 0.0001$). Together, these findings indicate that the elevated NFATc1 in aged HFSCs contributes markedly to the maintenance of the quiescent bulge signature.

To test the physiological relevance of these findings, we depilated young and aged animals, along with aged animals treated with VIVIT, and used qRT-PCR to measure the response of NFATc1 targets 48 h postdepilation. As shown in Fig. 6*C*, HFSCs from aged mice with VIVIT treatment had decreased mRNA levels of representative examples of the NFATc1 up-regulated genes and elevated expression of down-regulated genes. Overall, these findings suggest a heightened sensitivity of our differentially regulated age-related genes to fluctuations in NFATc1 activity.

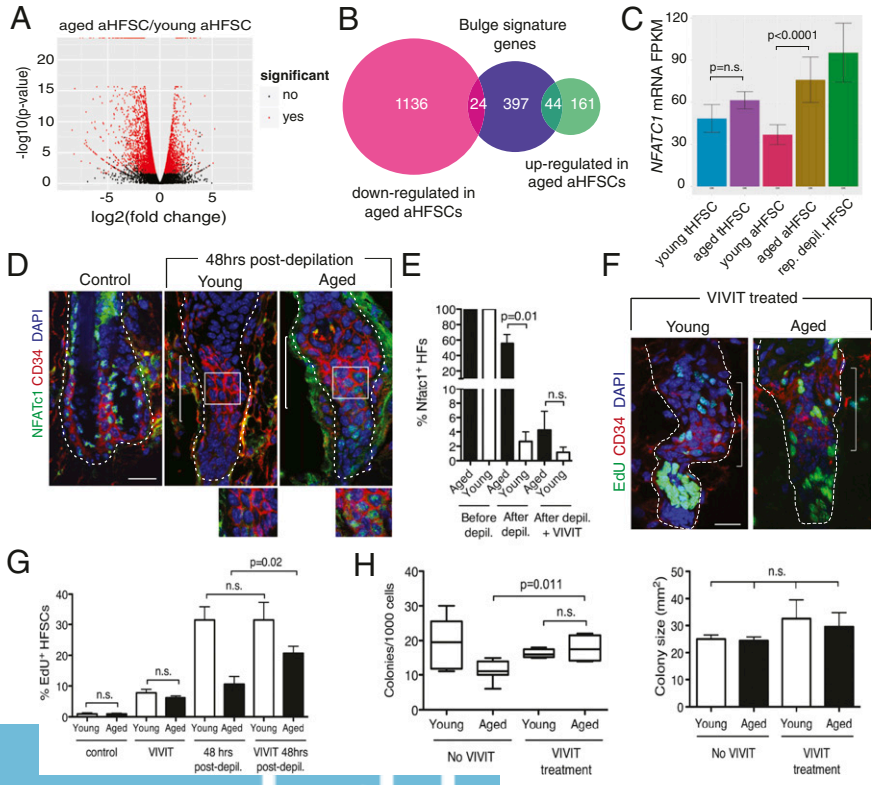

Fig. 5. Failure of *Nfatc1* to be down-regulated impedes the activation of aged HFSCs. (*A*) Volcano plot showing differentially regulated transcripts in aged vs. young HFSCs 48 h after depilation-induced activation (aged vs. young aHFSCs). (*B*) Diagram showing overlap of bulge signature gene set with age-related up- and down-regulated genes after depilation. (*C*) *Nfatc1* fragments per kilobase of exon per million reads (FPKM) levels from RNA-seq samples. n.s., not significant. Error bars represent both cross-replicate variability and uncertainty as estimated by Cufflinks (41). (*D*) Merged images of HFs before (control) and after depilation in young and aged animals. CD34 staining marks the bulge. Brackets in young and old HFs denote the bulge area. (Scale bar, 20 μM.) Squares indicates the region and their magnified *Insets* (1.5×) are below. (*E*) Quantifications of HFs with NFATc1$^+$ HFSCs (>4). Analyses were after depilation ± VIVIT treatment. Quantification $n = 3$ for each group. Data are mean ± SEM. (*F*) EdU incorporation in HFSCs from young and aged animals after treatment with VIVIT peptide. Brackets and CD34 staining mark the bulge. (Scale bar, 20 μM.) (*G*) Quantification of EdU incorporation by flow cytometry in HFSCs after VIVIT treatment. Data from Fig. 1*E* regraphed for comparison. $n = 4$ young; $n = 5$ aged. Data are mean ± SEM. (*H*) Quantification of CFE and colony size of HFSCs FACS-isolated and cultured 48 h after depilation from VIVIT-treated animals. $n = 4$ for each group. Data from Fig. 2*B* regraphed for comparison. Data are mean ± SEM.

Repetitive Use Renders Young HFSCs Old. Given our ability to detect a decline in the CFE of aged HFSCs that persists even when in vivo depilation-induced activation preceded the culturing, we wondered whether additional HFSC use might accentuate this defect, perhaps even exhausting their long-term self-renewal potential. To test this possibility, we subjected aged mice to multiple rounds of depilation (5–7, 42). Indeed after eight more hair cycles, their hair coats were significantly thinner and grayer than those of untreated aged and treated young mice (Fig. 7*A*). Notably, FACS quantifications revealed a nearly twofold decline in aged vs. young HFSC numbers following these multiple rounds of depilation (Fig. 7*B*). These differences were corroborated by immunofluorescence microscopy (*SI Appendix*, Fig. S7 *A* and *B*) underscoring a strong correlation between the age-related, depilation-enhanced decrease in hair regeneration and the concomitant decline in HFSC activation. We also documented a decline in melanocytes, which corroborated the hair graying in the repetitive depilation of young mice (*SI Appendix*, Fig. S7 *C* and *D*). Interestingly, this was not seen in the 24-mo-aged mice that we had used for our studies (*SI Appendix*, Fig. S1).

After eight rounds of depilation, young animals (now 7 mo old) had progressed through comparable numbers of hair cycles to untreated 22 to 24-mo-aged mice (Fig. 7*C*) (43). If HFSC use leads to a decline in SC activation potential, this should now be detectable in vitro. Indeed when isolated and cultured, these tHFSCs exhibited a greater than twofold decline in CFE and nearly threefold decline in colony size over equivalently aged mice that underwent only their normal four and not eight cycles (Fig. 7 *D* and *E*). These experiments suggest that increased use of HFSCs, at least in these wound-induced states, has a marked cell-autonomous effect on SC activation.

Finally we tested to see whether the HFSCs from the repetitively depilated SC niche had acquired other features of aged HFSCs. RNA-seq analyses of young tHFSCs after eight depilation-rounds revealed that the repetitively depilated younger HFSCs exhibited a program of gene expression that resembled the singly depilated 24-mo old HFSCs (aHFSCs) (*SI Appendix*, Fig. S5*A*). As shown in the diagram in Fig. 7*F*, ~35% of the NFATc1 target genes were shared among the differentially regulated gene sets after single depilation of aged mice and repetitive depilation of young mice. Additionally, when samples were clustered on the basis of NFATc1 target expression, the repetitively depilated HFSCs sample more closely resembled singly depilated aged HFSCs (*SI Appendix*, Fig. S6*E*).

Discussion

The Hair Cycle, SC Function, and Aging. One of the most striking phenotypes associated with old age is the decline in hair density. Our studies show that with age, domains of HF regeneration become more asynchronous and complex, periods of HF dormancy become longer, and periods of hair growth are shortened. These changes in dormancy and growth worsen beyond the initial loss of synchrony in the fourth hair cycle, suggesting that there are changes with age that contribute to the decline of HF activity. Surprisingly, HFSCs and melanocyte SCs from aging HFs were present in equivalent numbers to young HFs, and therefore changes in hair cycle activity were not based in a decline in the SC pool. Indeed, only when subjected to repetitive rounds of hair depilation did mice exhibit declines in both HFSCs and melanocyte SCs, manifested in hair thinning and graying. These results are akin to the reduced capacity of hematopoietic SCs to regenerate bone marrow after serial rounds of transplantation (44). Together, these findings suggest that for mice, in the absence of wounding, inflammation, and/or other assaults that enhance use, skin SCs are in adequate supply to fuel hair growth and pigmentation during the normal lifetime of the animal.

Our hair cycle activity analyses revealed that the anagen signal is still present in aged animals with a frequency and duration not dissimilar to young animals. This indicates that the delay in anagen entry is not due to a lack of stimulus, but rather a defect in the ability of HFSCs to initiate anagen effectively. Moreover, enhanced periods of HF dormancy even exist within triplets of tail skin HFs and thus extend beyond the macroenvironment to the microenvironment. Moreover, when given a strong stimulus (depilation) to proliferate, aged HFs progress uniformly to anagen, similarly to younger animals. These findings demonstrate that aged HFSCs are not irreparably damaged or senescent. We also saw no signs of inappropriate lineage commitment of progenitors (as seen in aged hematopoietic SCs). In these regards, the features of aging HFSCs appeared to be distinct from many other SC populations.

Self-Renewal vs. SC Activation. When mice were 12 mo of age, and progressing thereafter, the ability of their HFSCs to form colonies in vitro began to decline. Coincident with this decline was a progressive inability of HFs to fully regrow their hair coat during anagen (*SI Appendix*, Fig. S3). A priori, these could either be signs of a decline in self-renewal and/or an indication that aging HFSCs are intrinsically more resistant to activation/proliferation. Our findings provide evidence in support of both possibilities. Thus, CFE was not fully restored by depilation-induced stimulation of aged HFSCs, and aged HFSC-derived holoclones did show a decline in self-renewal after 10 passages in vitro or after multiple rounds of depilation in vivo. That said, the lion's share of the age-related hair defects were attributable to enhanced BMP/NFATc1 signaling within aged HFSCs.

The Influence of Intrinsic vs. Macroenvironmental Factors in HFSC Aging. Our parabiosis studies in which we exposed aged HFSCs to a young systemic environment gave an ~2X increase in CFE in vitro, which is comparable to the rejuvenation seen in neural SC populations after heterochronic parabiosis (9). Moreover, we did

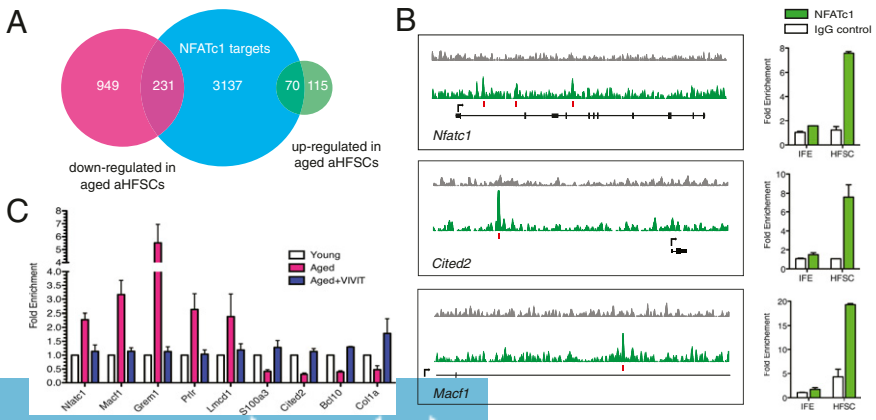

Fig. 6. NFATc1 targets are enriched in age-regulated genes. (*A*) Diagram showing overlap of NFATc1 targets (as identified by ChIP-seq) with age-related up- and down-regulated genes after depilation (as identified by RNA-seq). Up-regulated (70/185) $P = 1.6e\text{-}13$, down-regulated (231/1,180) $P = 0.0001$. (*B*, *Left*) ChIP-seq tracks of NFATc1-bound genes in HFSCs. Shown are representative examples *Nfatc1*, *Cited2*, and *Macf1* (gray is input control; green is NFATc1 ChIP-seq). *y* axis shows number of mapped reads at each genomic position. Red boxes mark peaks enriched in NFATc1 track. (*B*, *Right*) ChIP–qRT-PCR on independent samples from IFE and HFSCs. Green and white bars are NFATc1 and IgG control respectively. (*C*) qRT-PCR of representative NFATc1 target genes from HFSCs isolated by FACS from young and aged animals 48 h after depilation and aged animals treated with VIVIT 48 h after depilation. Data are mean ± SEM.

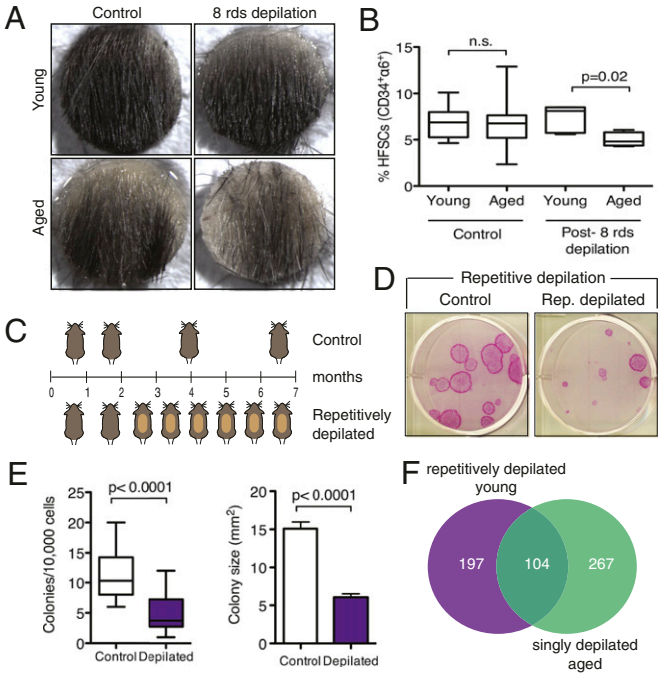

Fig. 7. HFs of repetitively depilated young mice share similarities with those of singly depilated aged mice. (*A*) Three-millimeter biopsy punches from back skins of young and aged control and repeatedly depilated animals. n = 5 young; n = 4 aged. rnd, rounds. (*B*) Quantification of $CD34^+$ $\alpha6$-$intergrin^+$ HFSCs in depilated animals by flow cytometry. Data are mean ± SEM. n.s., not significant. (*C*) Schematic diagram illustrating experimental timeline of depilation experiment. By 7 mo of age, C57BL6/J animals undergo three to four hair cycles. Animals that were repetitively depilated undergo eight hair cycles by 7 mo. (*D*) CFE after repetitive depilation. FACS-isolated HFSCs from control and repetitively depilated animals stained with Rhodamine B. (*E*) Quantification of CFE and colony size. n = 4 for each group. Data are mean ± SEM. (*F*) Diagram showing overlap (P = 7.02e-32) of NFATc1 target genes in repetitively depilated and singly depilated animals.

not see a deleterious effect on young HFSCs cultured from heterochronic vs. isochronic pairs. The specific improvement on aged HFSCs was intriguing in light of the elevated systemic GDF11 found in younger mice (11). TGF-β–signaling agonists have been shown to counteract intrinsic BMP signaling in HFSCs (45), which might be expected to preferentially benefit aged HFSCs. That said, the effects of heterochronic parabiosis in aged HFSCs in vivo were considerably less dramatic than seen either in vitro or compared with aged muscle SCs (satellite cells). Whether this reflects the more avascular nature of telogen HFs compared with muscle tissue (24, 46) awaits further investigation.

Modeling of HF cycling predicts that increases in inhibitor levels or decreases in excitatory signals can uncouple anagen synchrony, which then relies solely on intrinsic activation mechanisms to initiate anagen (25). Our data support this model, as aged HFSCs are more quiescent and harder to activate than their younger counterparts. Additionally, by dissecting the relative importance of extrinsic vs. intrinsic factors, we learned that the age-related decline in HFSC activity is due to a combination of both enhanced intrinsic sensitivity of HFSCs to BMP signaling and also an elevation in the local BMP levels within aged skin.

Mechanistic Insights Underlying the Age-Related Decline in HFSC Activity. Tracing mechanism, we were led to BMP-regulated *Nfatc1* and NFATc1 activity as a key contributor to the enhanced internal threshold that aging HFSCs display when challenged with anagen cues. By selectively forcing *Nfatc1* down-regulation (by blocking BMP activity) and/or NFATc1 (by blocking NFATc1 transcriptional activity), we provided compelling evidence that failure to properly down-regulate *Nfatc1*/NFATc1 during HFSC activation delays entry of aging HFs into the hair cycle. Collectively, these changes render aging HFSCs less competent to respond to anagen cues and proliferate. Although not sufficient on its own, local environment does contribute to this response, as BMP levels are elevated in the surrounding adipose tissue of aged mice. This imposes a higher environmental threshold for the activation of aged HFSCs, as revealed by our hair-plucking experiments. Overall, the outcome is a less coordinated, asynchronous anagen among neighboring HFs, a lethargic response of HFSCs to anagen activation cues and a thinning of hair density with age.

Finally, our ChIP-seq analyses revealed that of the changes in gene expression that are specific to aged HFSCs, ∼22% are NFATc1 targets. Moreover, many of these changes both in *Nfatc1*/NFATc1 and its target genes were recapitulated in HFSCs from younger animals that were subjected to repetitive depilation. These findings underscore a correlation between age-related decline in HFSC activity and enhanced HFSC use. Moreover, they highlight the special importance of enhanced BMP/NFATc1 signaling in explaining many of the age-related changes in HFSCs that we see.

In closing, a number of questions remain. Are there specific NFATc1 target genes which are key to the aging process, or do the constellation of age-related NFATc1 targets contribute collectively? Why are so many genes down-regulated in their expression in aged HFSCs? A number of these are NFATc1 targets, but is NFATc1 directly involved in their repression or are there other contributing factors that account for this? Do non-NFATc1–bound gene changes contribute to the intrinsic sensitivity that aged HFSCs seem to have in BMP/NFATc1 signaling? If so, how? Are there other factors that account for the use-related decline in self-renewal observed in long-term passaging in vitro or repetitive depilation in vivo, or will reducing BMP/NFATc1 signaling be sufficient to restore long term the youthfulness of aged HFSCs? Although beyond the scope of the present study, the answers to these questions will assuredly continue to bring interesting new twists to the fascinating process of aging in the skin.

Materials and Methods

Mice and Labeling Experiments. Aged (22–24 mo of age) C57BL6 animals were obtained from the National Institutes of Aging aged rodent colony and young animals (2–4 mo of age) were obtained from Jackson Laboratories. For animals from the aged rodent colony, we specified animals with "good hair coats" to avoid animals with clear signs dermatitis, fighting, scratching, and inflammation. Aged animals used in this study were also given a quick necropsy to discard animals with visible neoplasia. *K14-RFP* mice for in vitro colony growth studies were generated previously (27). Depilation of HFs was performed on anesthetized mice as described (42). For hair-plucking experiments, back skin hairs were clipped and the area of hairs to be plucked was marked using a template. Hairs were removed with forceps and monitored for hair growth. For EdU pulse experiments, mice were injected i.p. (50 μg/g) (Sigma-Aldrich) at times specified twice daily (12-h intervals). VIVIT (10 mg/kg) was injected i.p. once daily. Parabosis surgeries were performed as previously published (33). Parabiotic pairs were joined at 2 mo (young) and 24 mo (aged) of age and were kept 2 mo before analysis. For Noggin injections, recombinant mouse Noggin (R&D Systems) was injected intradermally with FluoSpheres (Invitrogen) for 3 consecutive days. EdU was administered 4 d after the last Noggin injection and animals were collected and EdU incorporation was scored in the hair germs of follicles near the injection site (marked by the FlouSpheres).

All animals were maintained in an American Association for the Accreditation of Laboratory Animal Care (AAALAC) International-approved Comparative Bio-Science Center at The Rockefeller University and procedures were performed using institutional animal care and use committee-approved protocols that adhere to the standards of the National Institutes of Health (NIH).

Hair Cycle Study. For the monitoring of the hair cycle, young (2 mo) and aged (24 mo) animals back skin hairs were trimmed with electric clippers and entry of HFs into anagen was observed by hair regrowth and by the appearance of darkening skin. Animals were checked on 3–4 d time intervals for 200 d and areas that entered into anagen were recorded. An independent set of young animals (n = 3) was used to monitor the second hair cycle and a second set

(n = 5) of young mice for cycles 3 and 4, for aged animals (n = 7). Mice were singly caged to avoid anagen as a result of wounding. Areas where hair growth was observed were retrimmed so future events could be observed. To monitor individual areas for anagen and telogen entry, the back skin was divided into 15 areas and the time intervals between the occurrences of anagen were determined.

For analysis of hair cycle data, regions of skin that had entered into anagen (based on pigmentation) were shaded on a to-scale map of back skin. These maps were scanned, digitized, and analyzed in a custom MATLAB (MathWorks)-based pipeline. Images of each time point were segmented using a watershed algorithm, and both the area and number of anagen regions were calculated and expressed as a percent of the 2D area of back skin, assumed to be the same for all mice. To compare the overall pattern and frequency of anagen in young and aged mice, segmented binary images of each time point were summed over the 200 d analyzed, such that the image intensity in a given region would correspond to the number of times it was found to be in anagen. The summed image was smoothed using a median filter with a 64 × 64-pixel window and displayed as a heat map.

RNA-Seq and Analysis. FACS-isolated HFSCs were sorted directly into TrizolLS (Invitrogen). Three animals were pooled per condition. RNA was purified using the Direct-zol RNA MiniPrep kit (Zymo Research) per manufacturer's instructions. Quality of the RNA for sequencing was determined using an Agilent 2100 Bioanalyzer; all samples used had RNA integrity numbers >8. Library preparation using the Illumina TrueSeq mRNA sample preparation kit was performed at the Weill Cornell Medical College Genomic Core facility (New York), and RNAs were sequenced on Illumina HiSEq 2000 machines. Alignment of reads was done using Tophat with the mm9 build of the mouse genome. Transcript assembly and differential expression was determined using Cufflinks with Refseq mRNAs to guide assembly (47). Analysis of RNA-seq data was done using the cummeRbund package in R (41). Transcripts regulated both greater than and less than 1.5-fold were used in Ingenuity Pathway Analysis (IPA) (Ingenuity Systems) to find enriched functional annotations.

Cell Culture. HFSC viability was determined using trypan blue (Sigma) staining using a hemocytometer after FACS isolation. Equal numbers of live cells were plated, in triplicate, onto mitomycin C-treated dermal fibroblasts in E-media supplemented with 15% (vol/vol) serum and 0.3 mM calcium (48). After 14 d in culture, cells were fixed and stained with 1% (wt/vol) Rhodamine B (Sigma). Colony diameter was measured from scanned images of plates using Image J and colony numbers were counted. For long-term passaging, 10 colonies were individually cloned and grown for 20 passages. Holocone formation was determined by growth and morphology of cells. To measure adhesion in CFE assays, HFSCs from *K14-RFP* mice were seeded onto feeder cells and allowed to adhere for 12 h. Media was changed and the number of cells in 10 independent fields was counted. For colony growth, individual colonies were imaged and cells were counted manually in the colonies. For BMP4-treatment experiments, freshly isolated HFSCs grown in vitro for 12 d were serum starved for 24 h then treated with recombinant Bmp4 (R&D Systems) at 100 ng/mL for 4 h. For Wnt treatment, cultures were treated with Wnt3a (R&D Systems) at 100 ng/mL for 12 h. Cells were collected directly in TRIzol (Invitrogen) and RNA was extracted for qRT-PCR (see *qRT-PCR*).

Histology and Immunofluorescence. Back skin tissues were embedded in optimal cutting temperature compound and frozen, cryosectioned (10–12 μm), and fixed in 4% (wt/vol) paraformaldehyde and then subjected to immunofluorescence microscopy or H&E staining as previously described (49). The antibodies (and their dilutions) used were as follows: anti-LHX2 (rabbit, 1:1,000; laboratory of E.F.), anti-CD34 (rat, 1:100; Pharmingen), anti-GFP (rabbit, 1:500; Invitrogen), anti-Ki67 (rabbit, 1:500; Novocastra), anti-NFATc1 (mouse, 1:500; Abcam), Id2 (rabbit, 1:1,000; BioCheck Inc.), KIT (rat, 1:1,000; BD Pharmingen), Keratin 5 (guinea pig, 1:500; laboratory of E.F.), MITF (mouse, 1:100; Abcam), TYRP1 [rabbit, 1:1,000; a gift from V. J. Hearing (National Cancer Institute, NIH, Bethesda, MD)]; Active Caspase-3 (Rabbit, 1:1,000; R&D Systems), and anti-pSmad1/5/8 (rabbit, 1:1,000, Millipore). Secondary antibodies conjugated to Alexa-488 and Alexa-647 (Molecular Probes) were used for imaging. Nuclei were stained using 4′,6-diamidino-2-phenylindole (DAPI). EdU staining was performed using the Click-iT EdU Alexa Fluor 488 Imaging Kit (Life Technologies) per manufacturer's instructions. MOM Basic Kit (Vector Laboratories) was used for blocking when primary antibodies were generated from mice (Nfatc1 antibody). Preparation of tail skin whole-mounts for imaging were done as described in ref. 50. Imaging was performed on Zeiss Axioplan 2, Zeiss Apotome, and Zeiss Inverted LSM 780 laser scanning confocal microscopes. Figures were prepared using ImageJ, Adobe Photoshop, and Illustrator CS5.

Flow Cytometry. Preparation of adult mice back skins for isolation of HFSCs and staining protocols were done as previously described (48). Briefly, s.c. fat was removed from skins with a scalpel, and skins were placed dermis side down on trypsin (Gibco) at 37 °C for 45 min. Single-cell suspensions were obtained by scraping the skin to remove the epidermis and HFs from the dermis. Cells were then filtered through 70-mm and then 40-mm strainers. Cell suspensions were incubated with the appropriate antibodies for 30 min on ice. The following antibodies were used for FACS: integrin α6 (eBiosciences, PE-conjugated), CD34 (eBiosciences, AlexaFluor 647-conjugated), and Sca-1 (eBiosciences, Alexa Fluor 700-conjugated). DAPI was used to exclude dead cells. Cell isolations were performed on FACSAria sorters running FACS-Diva software (BD Biosciences). FACS analyses were performed using LSRII FACS Analyzers and results analyzed with FlowJo. For EdU incorporation into HFSCs, staining was performed using Click-iT EdU Alexa Fluor 488 Flow Cytometry Kit (Life Technologies) per manufacturer's instructions.

qRT-PCR. RNA was purified from FACS-sorted cells by directly sorting into TrizolLS (Invitrogen) and purified using Direct-zol RNA MiniPrep kit (Zymo Research). Equivalent amounts of RNA were reverse-transcribed by Super-Script VILO cDNA Synthesis Kit (Invitrogen). cDNAs were normalized to equal amounts using primers against β-actin. cDNAs were mixed with indicated primers and Power SYBR Green PCR Master Mix (Applied Biosystems), and qRT-PCR was performed on an Applied Biosystems 7900HT Fast Real-Time PCR system. Primer sequences for qRT-PCR were obtained from Roche Universal ProbeLibrary.

ChIP-Seq and Data Analyses. All materials, methods, and sequencing have been described (23, 48). Independent immunoprecipitations were performed on FACS-sorted populations from female mice. Cells (20×10^6) were used for ChIP with anti-Nfatc1 antibody (Abcam, ab2796). Briefly, sorted cells were cross-linked in 1% (wt/vol) formaldehyde solution, resuspended, lysed, and sonicated to solubilize and shear cross-linked DNAs. For sonication, lysates were treated with 1% (vol/vol) Triton X-100 and then subjected to a Bioruptor Sonicator (Diagenode, UCD-200) according to a 30× regimen of 30-s sonication followed by 60-s rest. The resulting whole-cell extract was incubated overnight at 4 °C with 20 μL of Dynal Protein G magnetic beads (Invitrogen) which had been preincubated with ∼10 μg of the appropriate Ab. After ChIP, samples were washed, and bound complexes were eluted and reverse–cross-linked.

ChIP DNA was prepared for sequencing. Adaptor Oligo Mix (Illumina) was used in the ligation step. A subsequent PCR step with 25 amplification cycles added the additional Solexa linker sequence to the fragments to prepare them for annealing to the Genome Analyzer flow cell. After amplification, a range of fragment sizes between 150–300 bp was selected and the DNA was purified and diluted to 10 nM for loading on the flow cell. Sequencing was performed on the Illumina HiSEq 2500 Sequencer following manufacturer protocols.

ChIP-Seq reads were aligned to the mouse genome (mm9, build 37) using Bowtie aligner (49, 51). The SPP software (52) was used for calling peaks with data from ChIP input as controls. Annotated mouse RefSeq genes with a peak at their promoter proximal [±2 kb of transcription start site (TSS)], promoter distal (−50 to −2 kb of TSS), or gene body (+2 kb of TSS to ±2 kb of transcription end site) were considered as targets. The Multiple EM for Motif Elicitation (MEME) software suite (48, 53) was applied to 150-bp sequences around the ChIP-Seq peak summits for enriched motifs, with the program MEME for motif discovery and Motif Alignment and Search Tool (MAST) for motif scanning (P value <0.0005). ChIP-Seq signal tracks were presented by Integrative Genomics Viewer (IGV) software. ChIP-seq raw data have been deposted in the Gene Expression Omnibus database (www.ncbi.nlm.nih.gov/geo) (accession nos. GSE52328 and GSE48878).

Statistics. Student t test was used to determine the significance between two groups with Prism5 software. Box-and-whisker plots are used to describe the entire population without assumptions about the statistical distribution. For all statistical tests, the 0.05 level of confidence was accepted as a significant difference.

ACKNOWLEDGMENTS. We thank E.F. laboratory colleagues M. Kadaja, A. Asare, M. Genander, C. P. Lu, Y. C. Hsu, and N. Oshimori for intellectual input and suggestions; and N. Stokes, L. Polak, J. Dela Cruz-Racelis, and M. Nikolova for their assistance in the mouse and tissue culture facilities. We thank the Rockefeller University's Comparative Bioscience Center (AAALAC

International accredited) for care of mice in accordance with NIH guidelines, the Bioimaging Center for advice, and the Flow Cytometry staff for FACS sorting. We thank the Weill Cornell Medical School Genomics Center for sequencing and Dr. Olivier Elemento for advice on RNA-seq analysis. The research reported in this publication was supported by current grants from the National Institute of Arthritis and Musculoskeletal and Skin Diseases (to E.F.) and an Ellison Foundation Senior Scholar Award (to E.F). This research was conducted while B.E.K. was an Ellison Medical Foundation/American Federation for Aging Research Postdoctoral Fellow. E.F. is an Investigator of the Howard Hughes Medical Institute.

1. Sharpless NE, DePinho RA (2007) How stem cells age and why this makes us grow old. *Nat Rev Mol Cell Biol* 8(9):703–713.
2. Rossi DJ, et al. (2005) Cell intrinsic alterations underlie hematopoietic stem cell aging. *Proc Natl Acad Sci USA* 102(26):9194–9199.
3. Rossi DJ, et al. (2007) Hematopoietic stem cell quiescence attenuates DNA damage response and permits DNA damage accumulation during aging. *Cell Cycle* 6(19): 2371–2376.
4. Nishimura EK, Granter SR, Fisher DE (2005) Mechanisms of hair graying: Incomplete melanocyte stem cell maintenance in the niche. *Science* 307(5710):720–724.
5. Stolzing A, Scutt A (2006) Age-related impairment of mesenchymal progenitor cell function. *Aging Cell* 5(3):213–224.
6. Torella D, et al. (2004) Cardiac stem cell and myocyte aging, heart failure, and insulin-like growth factor-1 overexpression. *Circ Res* 94(4):514–524.
7. Conboy IM, et al. (2005) Rejuvenation of aged progenitor cells by exposure to a young systemic environment. *Nature* 433(7027):760–764.
8. Ruckh JM, et al. (2012) Rejuvenation of regeneration in the aging central nervous system. *Cell Stem Cell* 10(1):96–103.
9. Villeda SA, et al. (2011) The ageing systemic milieu negatively regulates neurogenesis and cognitive function. *Nature* 477(7362):90–94.
10. Brack AS, et al. (2007) Increased Wnt signaling during aging alters muscle stem cell fate and increases fibrosis. *Science* 317(5839):807–810.
11. Loffredo FS, et al. (2013) Growth differentiation factor 11 is a circulating factor that reverses age-related cardiac hypertrophy. *Cell* 153(4):828–839.
12. Chuttani A, Gilchrest BA (2010) *Skin* (John Wiley & Sons, Hoboken, NJ).
13. Alonso L, Fuchs E (2006) The hair cycle. *J Cell Sci* 119(Pt 3):391–393.
14. Cotsarelis G, Sun TT, Lavker RM (1990) Label-retaining cells reside in the bulge area of pilosebaceous unit: Implications for follicular stem cells, hair cycle, and skin carcinogenesis. *Cell* 61(7):1329–1337.
15. Tumbar T, et al. (2004) Defining the epithelial stem cell niche in skin. *Science* 303(5656):359–363.
16. Blanpain C, Lowry WE, Geoghegan A, Polak L, Fuchs E (2004) Self-renewal, multipotency, and the existence of two cell populations within an epithelial stem cell niche. *Cell* 118(5):635–648.
17. Morris RJ, et al. (2004) Capturing and profiling adult hair follicle stem cells. *Nat Biotechnol* 22(4):411–417.
18. Zhang YV, Cheong J, Ciapurin N, McDermitt DJ, Tumbar T (2009) Distinct self-renewal and differentiation phases in the niche of infrequently dividing hair follicle stem cells. *Cell Stem Cell* 5(3):267–278.
19. Hsu Y-C, Pasolli HA, Fuchs E (2011) Dynamics between stem cells, niche, and progeny in the hair follicle. *Cell* 144(1):92–105.
20. Plikus MV, et al. (2008) Cyclic dermal BMP signalling regulates stem cell activation during hair regeneration. *Nature* 451(7176):340–344.
21. Festa E, et al. (2011) Adipocyte lineage cells contribute to the skin stem cell niche to drive hair cycling. *Cell* 146(5):761–771.
22. Horsley V, Aliprantis AO, Polak L, Glimcher LH, Fuchs E (2008) NFATc1 balances quiescence and proliferation of skin stem cells. *Cell* 132(2):299–310.
23. Lien W-H, et al. (2011) Genome-wide maps of histone modifications unwind in vivo chromatin states of the hair follicle lineage. *Cell Stem Cell* 9(3):219–232.
24. Müller-Röver S, et al. (2001) A comprehensive guide for the accurate classification of murine hair follicles in distinct hair cycle stages. *J Invest Dermatol* 117(1):3–15.
25. Plikus MV, et al. (2011) Self-organizing and stochastic behaviors during the regeneration of hair stem cells. *Science* 332(6029):586–589.
26. Chase HB, Eaton GJ (1959) The growth of hair follicles in waves. *Ann N Y Acad Sci* 83:365–368.
27. Greco V, et al. (2009) A two-step mechanism for stem cell activation during hair regeneration. *Cell Stem Cell* 4(2):155–169.
28. Giangreco A, Qin M, Pintar JE, Watt FM (2008) Epidermal stem cells are retained in vivo throughout skin aging. *Aging Cell* 7(2):250–259.
29. Doles J, Storer M, Cozzuto L, Roma G, Keyes WM (2012) Age-associated inflammation inhibits epidermal stem cell function. *Genes Dev* 26(19):2144–2153.
30. Steingrímsson E, Copeland NG, Jenkins NA (2005) Melanocyte stem cell maintenance and hair graying. *Cell* 121(1):9–12.
31. Flores I, et al. (2008) The longest telomeres: A general signature of adult stem cell compartments. *Genes Dev* 22(5):654–667.
32. Barrandon Y, Green H (1987) Three clonal types of keratinocyte with different capacities for multiplication. *Proc Natl Acad Sci USA* 84(8):2302–2306.
33. McCay CM, Pope F, Lunsford W, Sperling G, Sambhavaphol P (1957) Parabiosis between old and young rats. *Gerontologia* 1(1):7–17.
34. Rando TA, Chang HY (2012) Aging, rejuvenation, and epigenetic reprogramming: Resetting the aging clock. *Cell* 148(1-2):46–57.
35. Conboy MJ, Conboy IM, Rando TA (2013) Heterochronic parabiosis: Historical perspective and methodological considerations for studies of aging and longevity. *Aging Cell* 12(3):525–530.
36. Molofsky AV, et al. (2006) Increasing p16INK4a expression decreases forebrain progenitors and neurogenesis during ageing. *Nature* 443(7110):448–452.
37. Park I-K, Morrison SJ, Clarke MF (2004) Bmi1, stem cells, and senescence regulation. *J Clin Invest* 113(2):175–179.
38. Aramburu J, et al. (1999) Affinity-driven peptide selection of an NFAT inhibitor more selective than cyclosporin A. *Science* 285(5436):2129–2133.
39. Rao A, Luo C, Hogan PG (1997) Transcription factors of the NFAT family: Regulation and function. *Annu Rev Immunol* 15:707–747.
40. Crabtree GR, Olson EN (2002) NFAT signaling: Choreographing the social lives of cells. *Cell* 109(Suppl):S67–S79.
41. Trapnell C, et al. (2012) Differential gene and transcript expression analysis of RNA-seq experiments with TopHat and Cufflinks. *Nat Protoc* 7(3):562–578.
42. Chen T, et al. (2012) An RNA interference screen uncovers a new molecule in stem cell self-renewal and long-term regeneration. *Nature* 485(7396):104–108.
43. Waghmare SK, et al. (2008) Quantitative proliferation dynamics and random chromosome segregation of hair follicle stem cells. *EMBO J* 27(9):1309–1320.
44. Harrison DE, Astle CM (1982) Loss of stem cell repopulating ability upon transplantation. Effects of donor age, cell number, and transplantation procedure. *J Exp Med* 156(6):1767–1779.
45. Oshimori N, Fuchs E (2012) Paracrine TGF-β signaling counterbalances BMP-mediated repression in hair follicle stem cell activation. *Cell Stem Cell* 10(1):63–75.
46. Yano K, Brown LF, Detmar M (2001) Control of hair growth and follicle size by VEGF-mediated angiogenesis. *J Clin Invest* 107(4):409–417.
47. Trapnell C, et al. (2010) Transcript assembly and quantification by RNA-Seq reveals unannotated transcripts and isoform switching during cell differentiation. *Nat Biotechnol* 28(5):511–515.
48. Nowak JA, Fuchs E (2009) Isolation and culture of epithelial stem cells. *Methods Mol Biol* 482:215–232.
49. Chang C-Y, et al. (2013) NFIB is a governor of epithelial-melanocyte stem cell behaviour in a shared niche. *Nature* 495(7439):98–102.
50. Braun KM, et al. (2003) Manipulation of stem cell proliferation and lineage commitment: Visualisation of label-retaining cells in wholemounts of mouse epidermis. *Development* 130(21):5241–5255.
51. Langmead B, Trapnell C, Pop M, Salzberg SL (2009) Ultrafast and memory-efficient alignment of short DNA sequences to the human genome. *Genome Biol* 10(3):R25.
52. Kharchenko PV, Tolstorukov MY, Park PJ (2008) Design and analysis of ChIP-seq experiments for DNA-binding proteins. *Nat Biotechnol* 26(12):1351–1359.
53. Bailey TL, et al. (2009) MEME SUITE: Tools for motif discovery and searching. *Nucleic Acids Res* 37(Web Server issue):W202-8.